Materials Physics and Mechanics 46 (2020) 70-87 Received: June 18, 2020

INVESTIGATION OF MULTISCALE MECHANISMS OF DYNAMIC DEFORMATION AND FRACTURE OF 1565 ALUMINUM ALLOY UNDER PLANE COLLISION AND HIGH-VELOCITY PENETRATION

Yu.I. Meshcheryakov[1*], G.V. Konovalov[1], A.K. Divakov[1], N.I. Zhigacheva[1], E.P. Osokin[2]

[1]Institute of Problems of Mechanical Engineering RAS, V.O. Bolshoi av., 61, Saint-Petersburg, 199178, Russia

[2]Central Research Institute of Constructional Materials "Prometei", Shpalernaya 14, Saint-Petersburg, 165114, Russia

*e-mail: ym38@mail.ru

Abstract. High strength 1565 aluminum alloy was tested within impact velocity range of 250-750 m/s in two schemes of shock loading: (i) under uniaxial strain conditions and (ii) in high-velocity penetration. The combination of load regimes allows the different stages of multiscale structure formation to be retraced. The intensity of macro-meso momentum exchange is found to be responsible for both resistance to spallation and high-velocity penetration. The overall impact velocity region is found to be subdivided by three sub-regions of different mechanisms of dynamic straining and scales. The strength behavior of material differs for different regions of impact velocities. Within impact velocity regions where the resistance to penetration increases, the spall strength decreases. The transition from one scale level to another is shown to be realized through the excitation of velocity oscillations at the mesoscale.

Keywords: aluminum alloy, spallation, high-velocity penetration, multiscale deformation, macro-meso momentum exchange, velocity oscillations

1. Introduction

Mechanics of dynamic deformation and fracture is developed in two approaches. The traditional mechanics grounded on the continuum approach deals with the representative volume and the concept of "point" for the effective elastic-plastic features inside the representative volume so the properties of individual dislocations and other defects are not essential. The basic mathematical apparatus for macroscale is the traditional apparatus of continuum elasticity, the theory of plasticity and creep. Various continuum approaches are being considered to address these issues, some of which are discussed in publications of Makarov [1,2], Baer and Trott [3], Briant [4], and Nesterenko [5]. As for the dynamic deformation and fracture, recent monograph of Kanel [6] can be considered as a total for this direction.

Further development of the mechanics of deformed solid supposes the incorporating of multiscale mechanisms of deformation and fracture. A critical issues of this study: (i) direct transition from atom-dislocation scale to macroscale is impossible [7,8]; (ii) microstructural investigations, even extremely of high scientific level, reflect the state of the structure in post-shocked specimens, which does not coincide with its state during the straining [9]. The

http://dx.doi.org/10.18720/MPM.4612020_8

concept of mesoscale has been suggested in 80-th in two scientific schools simultaneously but of different approaches. Tomsk's school supposes the formation of mesostructure in form of synergetic transition. As Makarov [1,2] points out, the shocked system evolves under loading so that its microstructure is capable of self-organizing into definite deformation regions – mesoparticles. The scientific school of Saint-Petersburg (Phys-Tech. Institute of A.F. Ioffe) proceeds from the physical mechanisms of mesostructure formation, specifically, as collectivization of polarized dislocation structure [10].

The first problem herein is how to describe a transition from one scale to another. Hard coupling between dynamic variables at the macroscale and atom-dislocation scale doesn't work. Specifically, well-known Eshby's formula [11]

$$\Delta\rho \equiv \rho_{ik}^{+} - \rho_{ik}^{-} = -\frac{1}{b} e_{ijl} \frac{\partial \varepsilon_{jk}}{\partial x_l},$$

which links a crystal curvature (macroscopic scale) and density of dislocations (microscale) can be used only for perfect crystals. Here ρ_{ik}^{+} and ρ_{ik}^{-} are the densities of positive and negative dislocations, b is the value of Burgers-vector, ε_{jk} is the component of deformation.

Adequate description of high-strain-rate processes is thought to be a combination of deterministic and statistical approaches. This means that instead of hard coupling, the sought transition must incorporate statistical variables which could provide a flexible linkage between neighbor scales.

According to another Saint-Petersburg's school, the shock-induced meso-structures are speculated to be nucleated in the form of short-living (150-200 ns) single-sign dislocation groups which in their scale belong to mesoscale-1 [12,13]. In turn, the process of nucleation and propagation of dislocation groups results in particle velocity fluctuations which are registered in the form of particle velocity distribution.

In parallel, the well-known scientific school of Sandia Laboratory (USA) performed a series of shock-wave experiments under uniaxial strain conditions with line-VISAR registration. These experiments reveal the large-scale velocity fluctuations at the mesoscale-2 (50-500 μm) for tantalum [14] and boron ceramics [15,16]. Specifically, these experiments reveal a direct coupling of the particle velocity distribution with the mechanism of spallation. Two-scale simulation of shock-wave propagation with taking into account the particle velocity distribution at the mesoscale has been conducted in [17,18]. The significant result of the simulation is a discovery of threshold particle velocity at which the material transits into a structure unstable state whilst the mechanism of dynamic deformation changes from uniform to turbulent.

As a rule, the investigations both theoretical and experimental, devoted to multiscale dynamic deformation deal with the shock-wave propagation initiated by loading under uniaxial strain conditions, which, however, cannot reveal the full picture of the dynamic deformation process. In contrast, the presented paper is devoted to studying the mesostructure formation in combined experiments. A critical step in having an efficient picture of multiscale processes is the parallel tests in two schemes of shock loading. The first scheme is the test under uniaxial strain conditions and the second scheme is the high-velocity penetration of elongated rigid rod. In the second scheme of shock tests, the impactor faces two mechanisms of resistance: (i) forehead resistance of plane nose of impactor and (ii) friction resistance of the lateral region of the rod. In shock tests under uniaxial strain condition, the target suffers only forehead resistance. A comparison of results in both schemes allows the role of macro-meso momentum exchange in multiscale deformation and fracture to be revealed.

2. Experimental technique

Shock tests under uniaxial strain conditions were conducted with a one-stage light gas gun of 37 mm barrel diameter. Plane targets were the discs of 52 mm in diameter and 7 mm thick. Data on dynamic strength of the material, including dynamic yield limit, spall strength, and threshold of structural instability are inferred from the temporal profiles of the free surface velocity, $u_{fs}(t)$, which are registered with the velocity interferometer. In Figure 1 the qualitative pattern for three random positions of wavefront in the heterogeneous medium is presented. The dotted lines correspond to the mean shock front position whereas meander lines present the random positions of separate pieces of the shock front. In this situation, the shock wave can be considered as a superposition of three modes of motion: (i) *mode-1* is the mean motion of plane shock front, (ii) *mode-2* is the fluctuative motions of separate pieces of mesoscale-1 relatively averaged motion of mesoscale-2 and (iii) *mode-3* is the fluctuative motions of separate pieces of mesoscale-2 relatively mean position of the shock front.

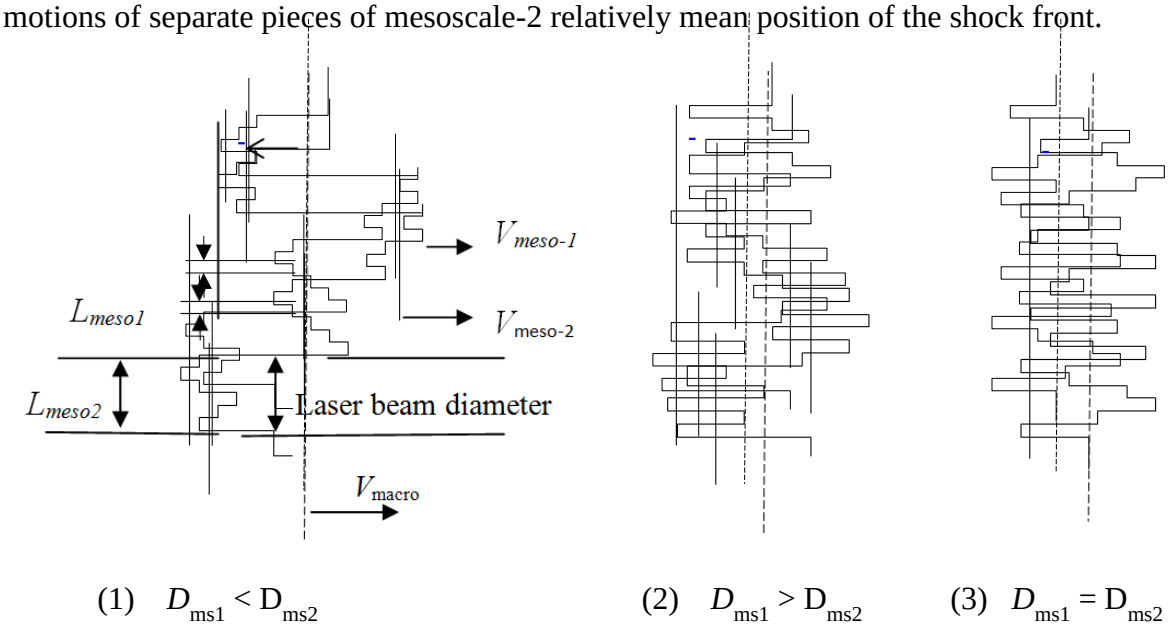

(1) $D_{ms1} < D_{ms2}$ (2) $D_{ms1} > D_{ms2}$ (3) $D_{ms1} = D_{ms2}$

Fig. 1. Qualitative pattern of velocity-space configurations of shock front for different relations between velocity dispersions at mesoscale-1 and mesoscale-2

The random motions of shock front pieces are quantitatively characterized by the velocity variance D (square root of the particle velocity dispersion). The interference technique allows both the mean particle velocity, u_{fs}, and particle velocity variance, D_{ms1}, to be registered in real-time [19,20]. Typical free surface velocity profile $u_{fs}(t)$ and particle velocity variance profile $D(t)$ for 1565 aluminum alloy are presented in Fig. 2. The free surface velocity profile characterizes a temporal history of mean particle velocity of dynamically deformed medium whereas the velocity variance $D_{ms1}(t)$, is a quantitative characteristic of scattering the particle velocity at the mesoscale.

For the steady shock waves, the particle velocity variance is maximum in the middle of the plastic front and decreases to zero to the top of the front. The measured with the interference technique value of the velocity variance characterizes an intensity of relaxation processes at the mesoscale-1. This means that to the top of the plastic front the relaxation processes at the mesoscale-1 are completed and transition to mesoscale-2 occurs.

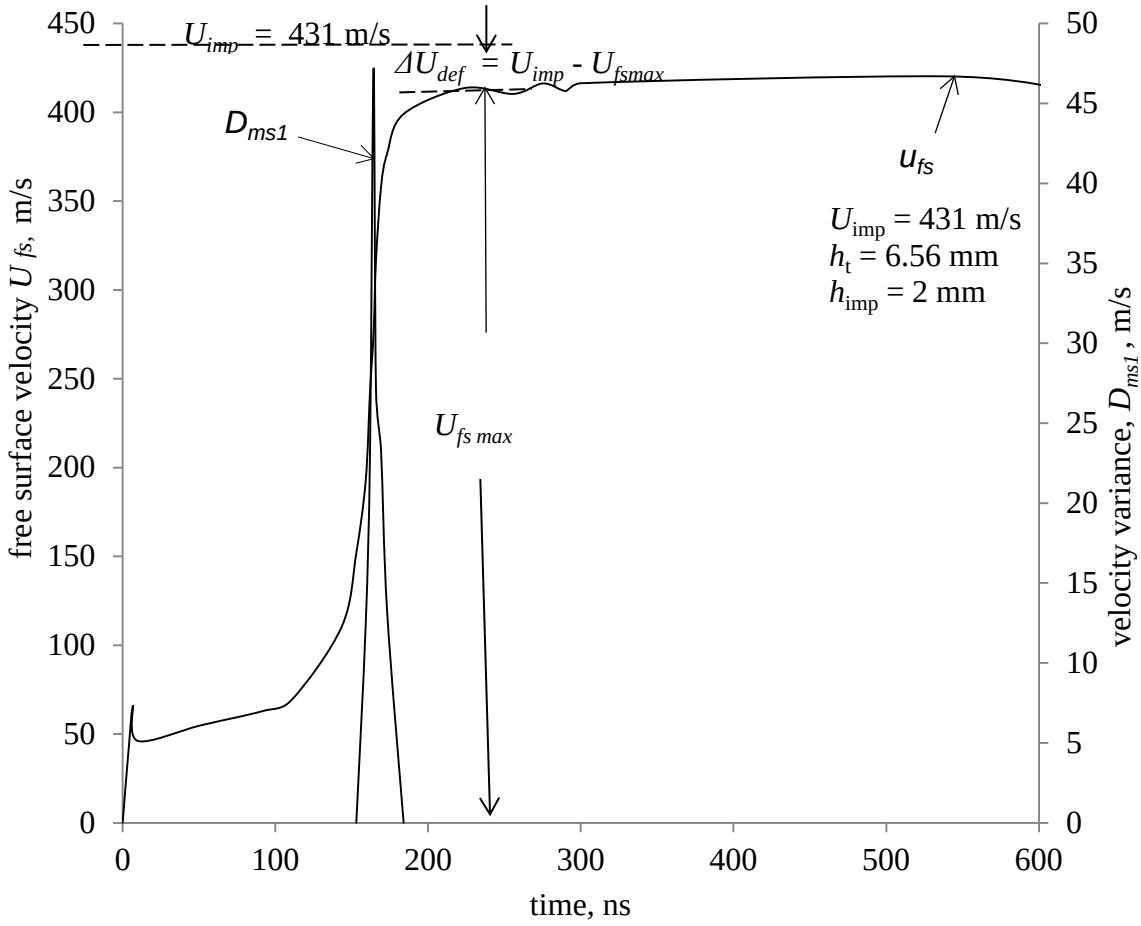

Fig. 2. Free surface velocity profile, u_{fs}(t), and velocity variance profile, D(t), at the impact velocity of 431 m/s

One of the important characteristics of multiscale dynamic deformation is the *defect of particle velocity*. It is determined in tests under uniaxial strain conditions as a difference between the velocity of the impactor and free surface velocity at the plateau of compressive pulse, $\Delta u_{def} = (U_{imp} - U_{fs}^{\max})$ (Fig. 2). This characteristic provides the quantitative data on momentum exchange between macroscale and mesoscale.

The second dynamic characteristic which reflects a transition of material into a structure-unstable state is the *threshold of structural instability* $U_{in.}$ It characterizes the beginning of shock-induced structural heterogenization of material. This characteristic can be obtained upon the series of the free surface velocity profiles registered under uniaxial strain conditions over the impact velocities range. The value of the free surface velocity $U_{fs} = f(U_{imp})$ at which the velocity defect begins to increase drastically is defined as the *threshold of structural instability*, U_{ins}. This characteristic has previously been introduced in [21-24]. It has been shown that material changes its structural state at the impact velocities which are higher than the threshold of structural instability. The threshold strain rate for such a kind of transition is determined for copper, steels, beryllium, aluminum alloys, and other materials.

Lastly, the third dynamic strength characteristic determined in tests under uniaxial strain conditions is the *spall strength* σ_{sp} which is often determined in the form of the so-called pull-back velocity, W at the back front of the compression pulse [25]. It should be noticed on the principal specifics of our experiments under uniaxial strain conditions. The laser beam

spot of interferometer focused on the free surface of the target is of the order of 50-70 μm. This means that the free surface profiles registered in our experiments reflect the response of only a single structural element of mesoscale-2 (see Fig. 1). The total response of target on impact can be obtained by averaging over the totality of mesoscale elements.

The high-velocity penetration tests were conducted with the same facility. To provide perpendicularity relatively plane target, the rod of 20 mm in length and 5 mm in diameter is mounted into polyvinyl carbonate sabot. The conditions for "*rigid rod and studied target"* are provided by using the high-strength 02Cr18Co9Mo5-VI maraging steel as a material for the rod. Typical penetration cavern in 1565 aluminum alloy target is shown in Fig. 3.

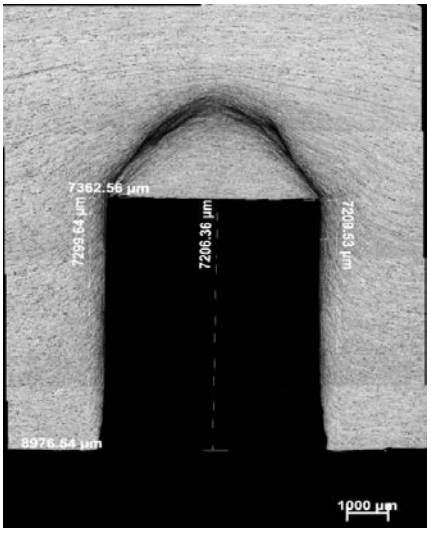

Fig. 3. Penetration cavern in 1565 aluminum alloy at the impact velocity of 577 m/s

The tests under uniaxial strain conditions provide the information on the character of spall fracture whilst the penetration tests allow the evolution of microstructure depending on the impact velocity to be retraced. In our experiments, the post shocked targets cut along the impact direction and after polishing and etching investigated with the optical microscope Axio-Observier Z-1m.

The quasistatic characteristics of the material are provided in Table 1.

Table 1. Mechanical characteristics of 1565 aluminum alloy

Alloy	Target thickness, mm	σ_b, MPa	σ_{02}, MPa	δ, %
Al. 1565	7	363	221	15.8

3. Experimental results and analysis

Structural instability and spall strength. A series of shocks under uniaxial strain conditions within impact velocity range of 250-750 m/s was performed. In Figure 4 the dependence of the value of maximum free surface velocity $U_{fs}^{\max}$ for 1565 aluminum alloy is plotted as functions of impact velocity. The free surface velocity corresponding to change of the slope of dependence $U_{fs}= f(U_{imp})$ is accepted to be the threshold of the structural instability of material. The critical changes of the slope of curve happen at the impact velocities of 440 m/s and 625.5 m/s (indicated by dotted lines).

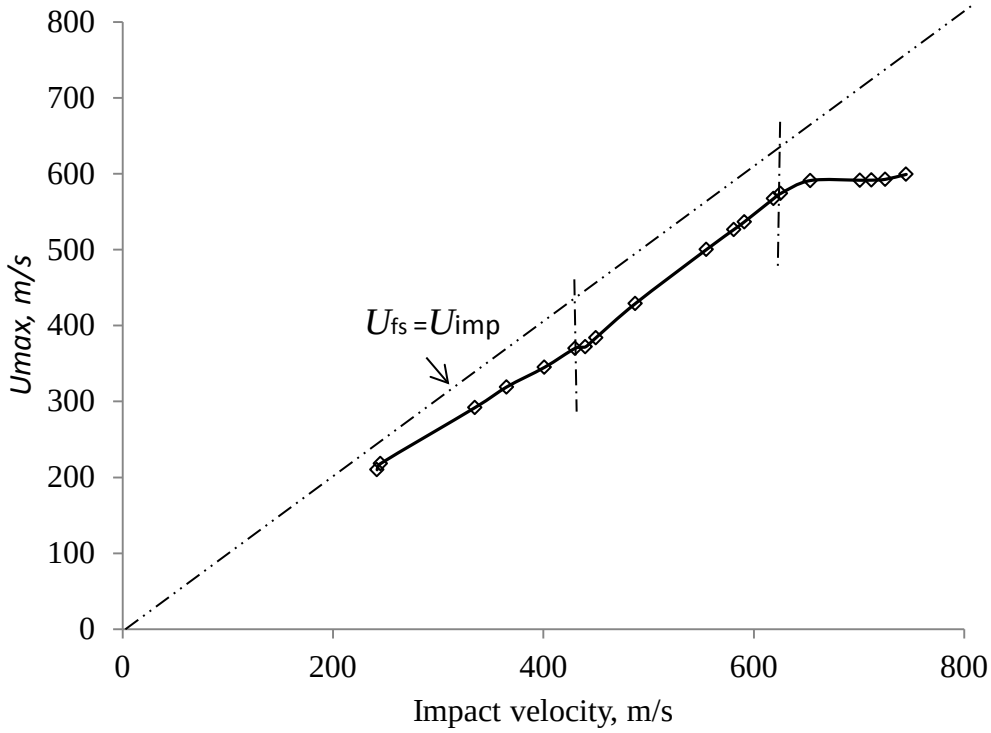

Fig. 4. Maximum free surface velocity $U_{fs}^{\max}$ versus impact velocity

The second dynamic strength characteristic of materials registered in tests under uniaxial strain conditions is the spall strength. Whereas the threshold of structural instability characterizes the dynamic strength of the material under compression, the spall strength is the tensile strength characteristic.

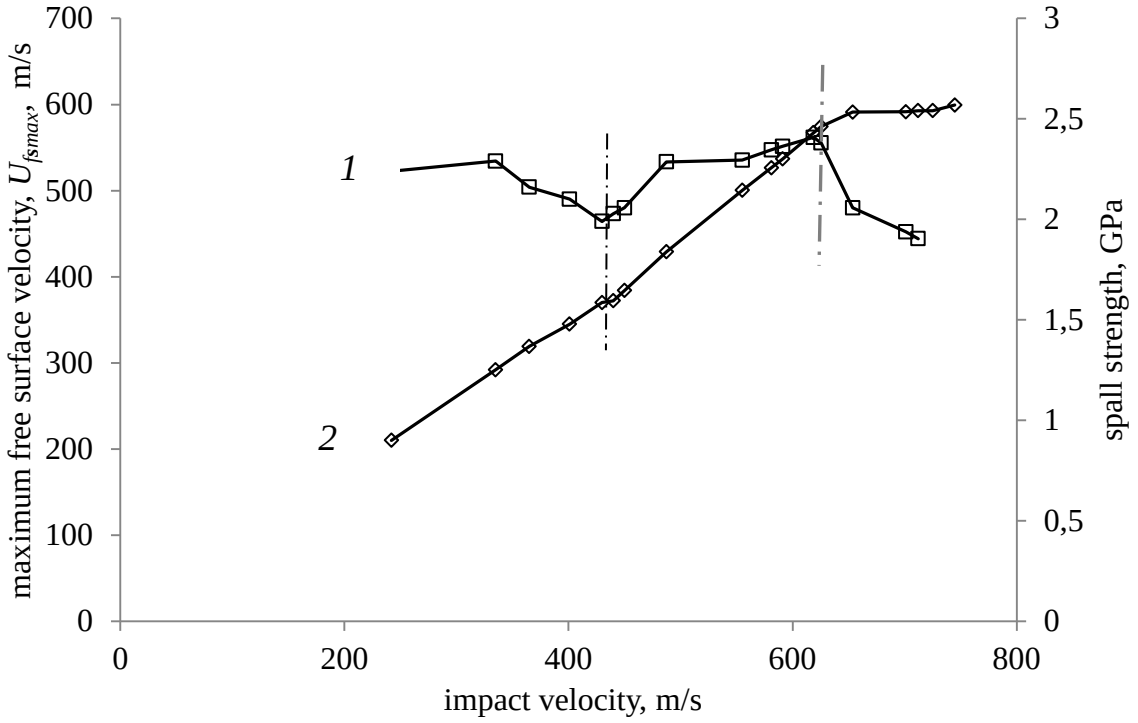

Fig. 5. Spall strength *(1)* and maximum free surface velocity $U_{fs}^{\max}$ (*2*) versus impact velocity

In Figure 5 the dependencies of maximum free surface velocity $U_{fs}^{\max}$ and spall strength on the impact velocity are plotted together. The breaks at the curves happen at the identical impact velocities indicated with dotted lines This means that the internal processes responsible for multiscale dynamic deformation and strength for both regimes of loading are mutually related.

Structural instability threshold and high-velocity penetration. Resistance to high-velocity penetration is characterized, firstly, by the value of penetration depth, L, and secondly, by the slope of curve $L = f(U_{imp})$, namely: (i) the smaller penetration depth L, the higher resistance to penetration and (ii) the smaller the slope of curve $L = f(U_{imp})$, the higher the resistance to penetration.

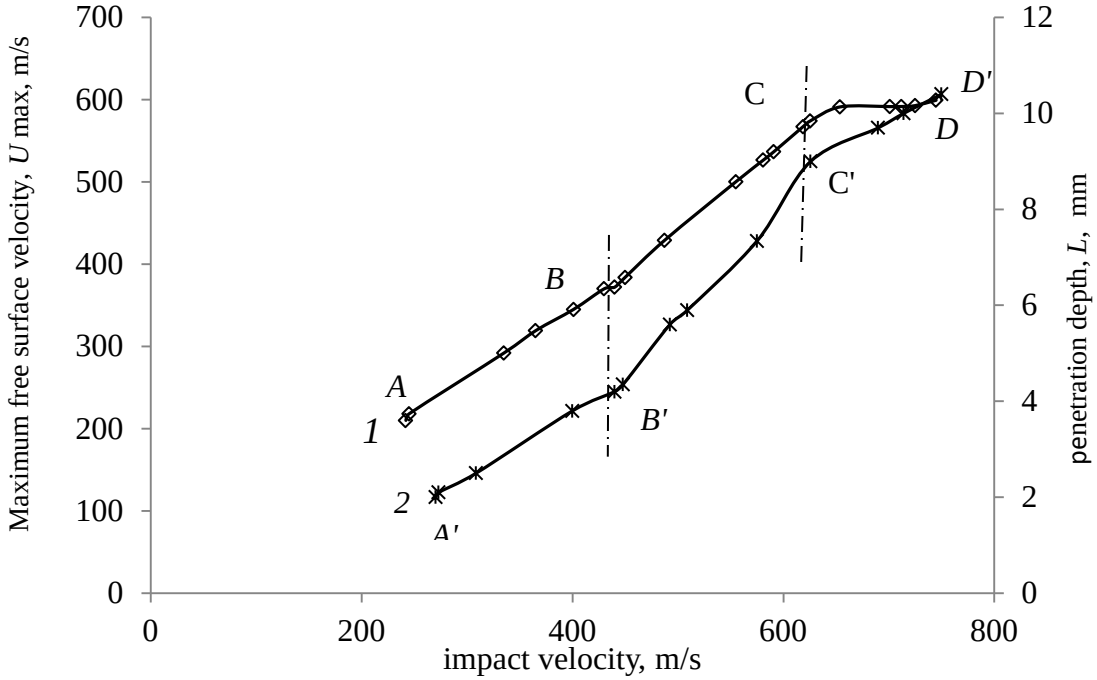

Fig. 6. Maximum free surface velocity $U_{fs}^{\max}$ (*1*) and penetration depth L (*2*) versus impact velocity

In Figure 6 the dependencies of $U_{fs}^{\max} = f(U_{imp})$ and penetration depth $L = f(U_{imp})$ on the impact velocity are plotted together. Within impact velocities from 241.9 m/s to 750 m/s the penetration curve suffers the breaks at the impact velocities of 440 m/s (position *B'*) and 625.5 m/s (position *C'*). The relation between the rate of change of structural instability threshold and rate of change of penetration depth can be summering as following:

1). Impact velocity region of 241.9-625.5 m/s: $\frac{dU_{\max}^{AB}}{du} < \frac{dU_{\max}^{BC}}{du}$; $\frac{dL_{A'B'}}{du} < \frac{dL_{B'C'}}{du}$.

2). Impact velocity region of 440-750 m/s: $\frac{dU_{\max}^{CD}}{du} < \frac{dU_{\max}^{BC}}{du}$; $\frac{dL_{C'D'}}{du} < \frac{dL_{B'C'}}{du}$.

The inequality $\frac{dL_{A'B'}}{du} < \frac{dL_{B'C'}}{du}$ means that resistance to penetration decreases after an impact velocity of 440 m/s. Within the impact velocity region from 625.5 m/s to 750 m/s, after point *C'*, an analogous inequality takes place: $\frac{dL_{C'D'}}{du} < \frac{dL_{B'C'}}{du}$, which means that

resistance to penetration after impact velocity of 625.5 m/s again increases. It may be concluded that the processes responsible for structural instability of material and high-velocity penetration are mutual related. The change of slope of curve $U_{fs}^{\max} = f(U_{imp})$ correlates with the behavior of the defect of particle velocity Δu_{def}.

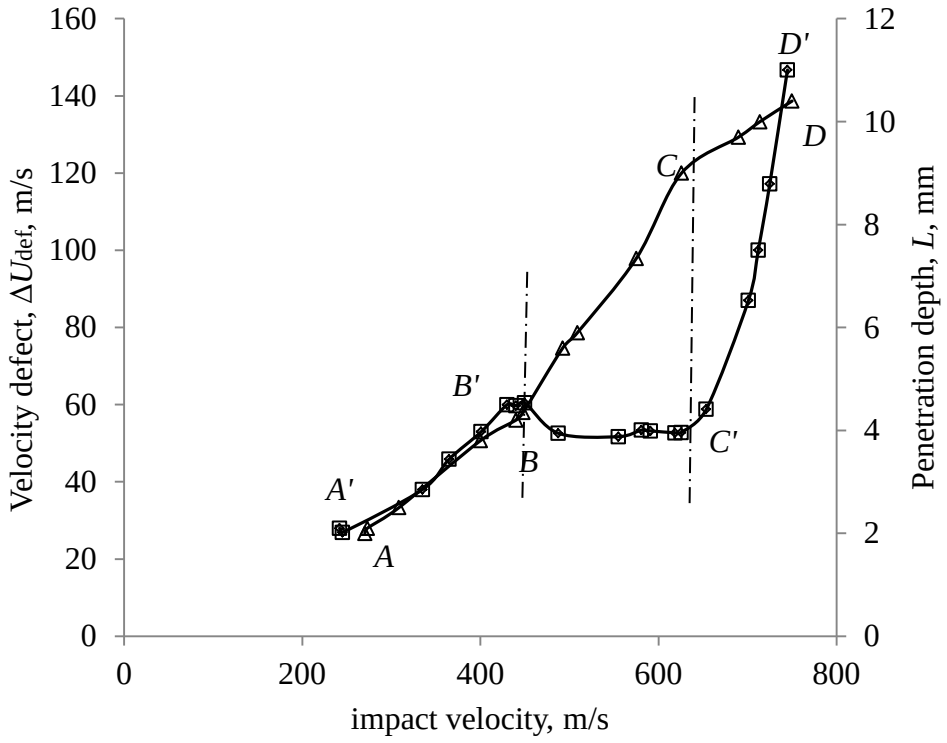

Fig. 7. Penetration depth L (*1*) and velocity defect Δu_{def} (*2*) versus impact velocity

Resistance to high-velocity penetration and velocity defect. Figure 7 shows that the behavior of the velocity defect correlates with the behavior of penetration depth. The relations between the rate of change of velocity defect and rate of change of penetration depth can be summering as following:

1) Impact velocity region of 241.9-625.5 m/s: $\frac{d\Delta u_{A'B'}^{def}}{du} > \frac{d\Delta u_{B'C'}^{def}}{du}$, $\frac{dL_{AB}}{du} < \frac{dL_{BC}}{du}$.

2) Impact velocity region of 440-750 m/s: $\frac{d\Delta u_{C'D'}^{def}}{du} > \frac{d\Delta u_{B'C'}^{def}}{du}$. $\frac{dL_{CD}}{du} < \frac{dL_{BC}}{du}$.

Within the upper region of impact velocities *CD*, the resistance to penetration increases. It should be noted that 1565 aluminum alloy has been specially created for working at high-velocity region of dynamic loadings. The beaks for both curves happen at identical impact velocities (indicated with vertical dotted lines).

Spall strength, resistance to high-velocity penetration, and velocity variance. It is thought to be very interesting to compare the spall strength and resistance to penetration behavior for different regions of impact velocities. In Figure 8 the penetration depth curve $L = f(U_{imp})$ for 1565 alloys is plotted together with the dependence for spall strength $W = f(U_{imp})$. A comparison of curves shows that the correlation between processes really exists. Dependence $W = f(U_{imp})$ based on tests under uniaxial strain conditions suffers two

breaks: at the impact velocities of 440 m/s and 625.5 m/s. The dependence of penetration depth $L = f(U_{imp})$ also suffers two breaks: at the impact velocities of 440 m/s and 608 m/s. The critical change of slope for penetration dependence happens at the velocity where the break for dependence $W = f(U_{imp})$ occurs (dotted lines in Fig. 8). Such behavior of curves evidences the common mechanism of structure behavior in tests under uniaxial strain conditions and high-velocity penetration. The breaks at the high region of impact velocities in both loading schemes also happen at close impact velocities: 625.5 m/s in-plane tests and 608 m/s in penetration tests. This means that both breaks are of the same nature.

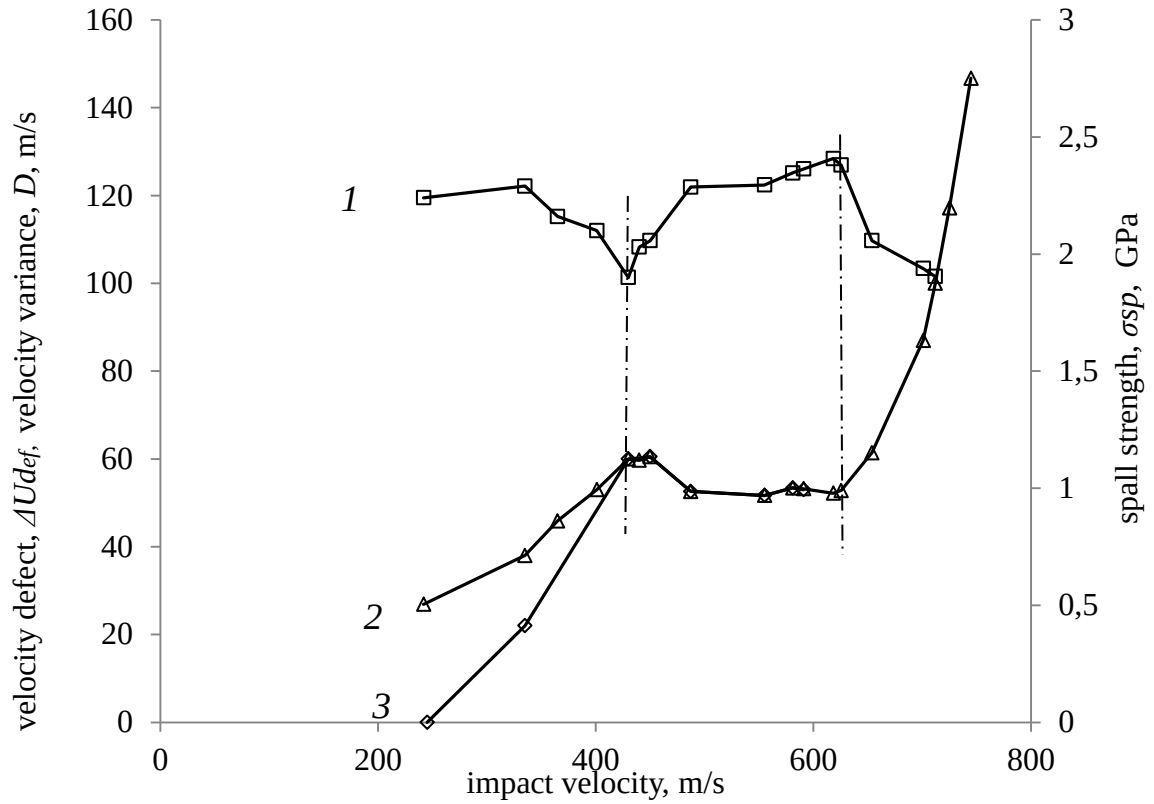

Fig. 8. Spall strength, W, (*1*), velocity defect, ΔU_{def}, (*2*) and velocity variance, D, (*3*) versus impact velocity

Now let us consider a correlation between spall strength behavior and resistance to penetration over the impact velocity regions:

1) *Penetration*:

a) Impact velocity region 241.9 - 625.5 m/s: $\frac{dL_{AB}}{du} < \frac{dL_{BC}}{du}$.

b) Impact velocity region 440 - 750 m/s: $\frac{dL_{CD}}{du} < \frac{dL_{BC}}{du}$.

2) *Spallation:*

a). Impact velocity region 241.9 - 440 m/s: $\frac{dW_{A'B'}}{du} < 0$.

b) Impact velocity region 440 - 625.5 m/s: $\frac{dW_{A'B'}}{du} \simeq 0$.

c) Impact velocity region 625.5 - 750 m/s: $\frac{dW_{A'B'}}{du} < 0$.

Within impact velocity region of 241.9 - 625.5m/s, the slope of penetration depth curve changes at point *B'*: $\frac{dL_{A'B'}}{du} < \frac{dL_{B'C'}}{du}$, which means that the resistance to penetration within impact region *A'B'* of the curve (*2*) is higher as compared to that for piece *B'C'*. At the same time, the spall strength within the same impact velocity region shows the opposite trend. Within the piece *AB* the spall strength decreases from 137.8 m/s to 117.3 m/s. After point *B*, within piece *BC*, $\frac{dW_{BC}}{du} \simeq 0$, which means that spall strength is approximately constant. The critical changes in both curves happen at an impact velocity of 440 m/s. The analogous situation is seen after the second critical impact velocity of ~ 625.5 m/s - within piece *C'D'* the slope of penetration curve (*2*) decreases: $\frac{dL_{C'D'}}{du} < \frac{dL_{B'C'}}{du}$, i.e. the resistance to penetration within region *C'D'* increases whereas $\frac{dW_{CD}}{du} < 0$, which means that spall strength in this region of strain rates decreases.

Thus, within impact velocity range of (241.9 - 750) m/s the strength behavior of 1565 aluminum alloy in two schemes of shock loading turns out to be opposite – *when resistance to penetration increases, the spall strength decreases.*

In Figure 8, besides the spall strength and penetration depth, the dependence for velocity defect on the impact velocity is provided. In our experiments, the mean particle velocity, *u*, and velocity variance, D_{ms1}, are registered in the form of temporal profiles (see Fig. 2). Independent measuring the impact velocity allows three shock-wave characteristics to be determined in real-time. The breaks at curves are seen to occur at identical impact velocities. The spall strength is seen to decrease when velocity defect increase (regions *A'B'* and *C'D'*). At the same time, the spall strength is *practically constant* when the velocity defect remains constant.

Such a kind of behavior of spall strength can be explained from the position of macro-meso energy and momentum exchange which is described by the following equation [26]:

$$\Delta u_{def} = -\frac{1}{2}\frac{\partial D^2}{\partial u}. \tag{1}$$

The left-hand side of this equation, the velocity defect, characterizes the momentum which transferred from macroscale to mesoscale. This transference is realized due to a change of the mesoparticle velocity dispersion, D^2. Eq. (1) can be written in the form

$$\Delta u_{def} = -D\frac{dD/dt}{du/dt}. \tag{2}$$

When the rate of change of the velocity variance equals to rate of change of mean particle velocity.

$$\frac{dD}{dt} = \frac{du}{dt}, \tag{3}$$

the velocity defect equals velocity variance:

$$\Delta u_{def} = -D. \tag{4}$$

This situation corresponds to the equilibrium regime of multiscale dynamic deformation and corresponds to the middle region of impact velocities *B'C'* in Fig. 8. In the case of

uniaxial straining, the deformations at the macroscale and mesoscale equal, respectively, Eq. (2) can be written in the terms of strain and strain rate:

$$\Delta\varepsilon_{def} = -\varepsilon_{ms}\frac{d\varepsilon_{ms}/dt}{d\varepsilon_{mc}/dt}. \quad (5)$$

Here $\Delta\varepsilon_{def}$ is an additional macroscopic deformation resulted from the interscale momentum exchange, $d\varepsilon_{ms}/dt$ is the strain rate at the mesoscale, and $d\varepsilon_{mc}/dt$ is the strain rate at the macroscale. When

$$d\varepsilon_{mc}/dt = d\varepsilon_{ms}/dt \quad (6)$$

all change of deformation at the macroscale resulted from interscale momentum exchange is determined by the value of deformation at the mesoscale $\Delta\varepsilon_{def}$=-ε_D. In shock experiments, the directly registered characteristics are the free surface velocity, u_{fs} velocity defect, Δu_{def}, and velocity variance, *D*. At the same time, the physical meaning of the processes may be understood from Eq. (6) which implies the equality of local strain rate and macroscopic strain rate. As distinct from the macroscopic strain rate, the local strain rate cannot be directly determined in dynamic experiments. Therefore, Eq. (4) can serve as a reliable feature for the equality of local and macroscopic strain rates.

The meso-macro energy exchange can explain a non-monotonous behavior of spall strength depending on the strain rate. The power balance at the spalling zone can be written in the form:

$$\frac{1}{2}\rho C_p u^2 = \frac{1}{2}\eta\frac{(u+\Delta u_{def})}{h}u. \quad (7)$$

Here ρ is a density of the material, C_p is the velocity of the shock wave, η is dynamic viscosity of deformed material and *u* is the particle velocity. The left-hand side of Eq. (7) characterizes the power which is brought into the spalling zone from the shock wave. The right-hand side of the equation describes the loss of power due to the normal rupture of material under tension at the spalling zone and reflects a motion of spall surfaces in opposite directions. As particle velocity is current changes owing to meso-macro energy exchange mechanism the mean particle velocity for this item includes the velocity defect Δu_{def}, and the total strain rate at the spalling zone equals:

$$\frac{d\varepsilon_1}{dt} = \frac{u+\Delta u_{def}}{h}, \quad (8)$$

where *h* is the width of the spalling zone. From (7) and (8) one obtains

$$h = \left(\frac{\rho C_0}{\eta} - \frac{\Delta u_{def}}{h}\frac{1}{u}\right)^{-1}. \quad (9)$$

Time for spallation can be determined as

$$\tau_f = \frac{h}{u} = \left(\sigma - \eta\frac{\Delta u_{def}}{h}\right)^{-1}, \quad (10)$$

where $\sigma = \rho C_p u$. Eq. (10) can be rewritten in the form:

$$\left(\sigma - \eta\frac{\Delta u_{def}}{h}\right)\tau_f = 1. \quad (11)$$

Generalization of this equation

$$\int_0^{\tau_f} \left(\sigma - \mu \frac{\Delta u_{def}}{h} \right) dt = 1 \qquad (12)$$

can be considered as a *dynamic fracture criterion* that takes into account the meso-macro momentum exchange. In this equation, the value σ has a meaning of the spall stress which characterizes the resistance of the material to spallation. It is seen that spall stress decreases when the velocity defect increases.

4. Microstructural investigations

The initial structure of 1565 aluminum alloy contains elongated grains, i.e. texture (Fig. 9*a*). To understand the multiscale mechanisms of strength behavior of alloy in different regions of impact velocities it was thought to be appropriate to compare the microstructural data for different regions of impact velocity with the dependencies of penetration over the same regions. The overall region of impact velocities in accordance with Fig. 8 is subdivided into three sub-zones.

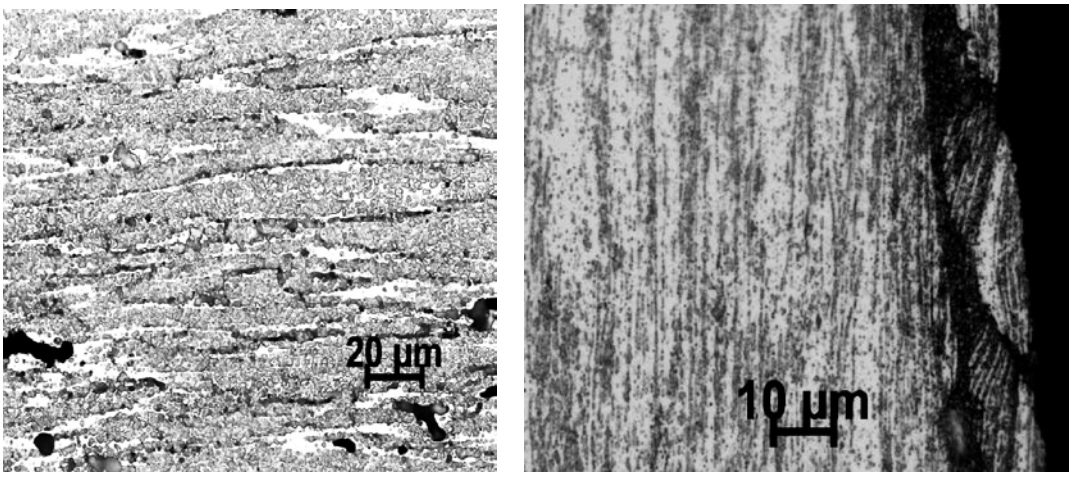

a) *b)*

Fig. 9. Initial structural states of 1565 aluminum alloy (*a*), micro shears, and fault structures in post shocked specimen (*b*)

The main feature of post-shocked specimens is the presence of numerous micro shears of 3-10 μm length oriented along the shock direction. The micro shears are nucleated owing to mass velocity pulsations at small impact velocities. Theoretical [12,13] and experimental [4] investigations of multiscale mechanisms of dynamic deformation show that the behavior of mesostructure under dynamic loading can be characterized by the presence of short-living pulsations of particle velocity. The motions of mesostructural elements in form of single-sign dislocation groups create the short-living mass velocity pulsations of $\Delta t \approx$ 150-200 ns duration. The velocity interferometer registers the particle velocity distribution in form of velocity variance *D*. In the case of 1565 aluminum alloy, the maximum value of velocity variance at the mesoscale-1 equals $D = 4.5 \cdot 10^3$ m/s (see Fig. 2), from where the mean displacement equals:

$L = D \cdot \Delta t = 4.5 \times 10^3 \cdot 2 \times 10^{-7} = 9 \times 10^{-4}$ cm.

In their dimensions, the displacements belong to mesoscale-1 (1-10 μm). The decreasing the distance to the bank of cavern density of micro shears increases.

Another structural element proper to high-velocity penetration is the so-called fault structures at the bank of the cavern. In Figure 9*b* a complex morphology of fault structure is presented – inside each cell a family of shear bands is incorporated.

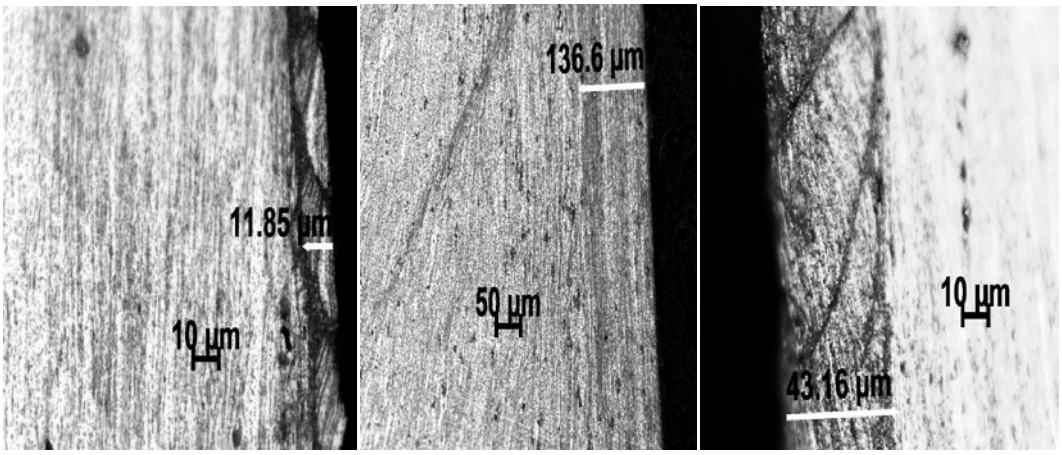

a) Region *AB* *b*) Region *BC* *c*) Region *CD*

Fig. 10. Three regions of lateral structure in 1565 aluminum alloy target after penetration

In Figure 10 the three states of structure for different regions of impact velocity are provided. Within the regions *AB* and *CD*, the specific feature of post shocked specimens is the presence of regular fault structures at the bank of the cavern and uniform deformation picture inside the region *BC*. The width of the region occupied by fault structures depends on impact velocity: within region *A* the width of the fault structure zone equals 7-12 μm whereas at the region *CD* the width of the zone increases up to 47-50 μm. A comparison with the reciprocal regions for high-velocity penetration curve (Fig. 8) shows that resistance to penetration at these regions increases. Within region *BC* where the regular faults are absent, the post-shocked structure is uniform whilst the resistance to penetration decreases. From the point of view of resistance to penetration, the 1565 aluminum alloy turns out to be more preferable at the upper region of impact velocities. At the same time, the spall strength of 1565 alloy at the upper region of impact velocities decreases (see Fig. 8).

5. On the resonance excitation of mesoscale

In the light of the above experimental results, three questions arise: (i) what is the physical mechanism responsible for nucleation of fault structures, (ii) what parameters of shock wave determine the dimensions of fault structures, (iii) what is the physical mechanism for transition from one scale to another. To answer the questions we consider propagation of plane shock wave in a relaxing medium.

In the case of a steady shock wave, two important relationships have previously been found. The first of them ties the particle velocity variance, *D*, and strain rate [26]:

$$D = R\frac{\partial\varepsilon(t)}{\partial t}\ . \qquad (13)$$

Here *D* is the velocity variance which is the quantitative characteristic of the intensity of the particle velocity chaotic pulsations in dynamically deformed solid, $\frac{d\varepsilon}{dt}$ is the strain rate and *R* is the proportionality coefficient. An analogous relationship is known to exist in turbulence where the intensity of turbulent pulsations is proportional to particle acceleration [27].

Eqs. (1), (13) determine the character of coupling between macroscopic and mesoscopic scales of dynamic straining. We use Eqs. (1) and (13) for a description of the response of relaxing medium on shock loading.

In the case of one-dimensional propagation of shock wave, the balance equations for momentum conservation and medium continuity take the form

$$\rho u_t - \sigma_x = 0; \tag{14}$$

$$u_x - \varepsilon_t = 0. \tag{15}$$

The constitutive equation for a relaxing medium introduced by Duvall [28] and Taylor [29]:

$$\sigma - \rho C_l^2 \varepsilon = -2\mu\varepsilon^p \tag{16}$$

or in differential form

$$\sigma_t - \rho C_l^2 \varepsilon_t = -F\,. \tag{17}$$

Here C_l is the longitudinal sound velocity, μ is the shear modulus, and the relaxation function

$$F = 2\mu\frac{\partial\varepsilon^p}{\partial t} \tag{18}$$

is determined through the plastic strain rate which, in turn, is determined by Orowan's equation for density and velocity of dislocations $\frac{d\varepsilon^p}{dt} = bN_dV_d$. As distinct from Duvall-Taylor approach, in the present investigation the stress relaxation in the dynamically deformed medium is accepted to be realized only through the motion of elementary carriers of deformation at the mesoscale. Dislocations and other carriers of the deformation of atom-dislocation scale provide the formation and motion of mesoparticles whereas the mesoparticles play a role of self-consistent carriers of deformation. In this situation, the stress relaxation is determined only by the velocity defect:

$$\frac{\partial\varepsilon^p}{\partial t} = \frac{1}{C_l}\frac{\partial(\Delta u_{def})}{\partial t}. \tag{19}$$

The advantage of such an approach is that the relaxation model doesn't incorporate the parameters of dislocations, such as density and velocity of dislocations which cannot be controlled under conditions of dynamic straining. As distinct from the dislocation structure, defect of particle velocity can be registered in real-time (see Fig. 2). In this case, the relaxation function takes the form:

$$F = \frac{2\mu}{C_l}\frac{\partial(\Delta u_{def})}{\partial t}. \tag{20}$$

The equation system (14) - (17)) can be reduced to second-order differential equation

$$\rho\varepsilon_{tt} - \sigma_{xx} = 0. \tag{21}$$

Substitution of (1) and (13) into (19) yields:

$$\frac{\partial\varepsilon^p}{dt} = \left(R^2/C_l^2\right)\frac{\partial^2\varepsilon}{\partial t^2}. \tag{22}$$

Then Eq. (21) is reduced to:

$$\varepsilon_{tt} - \rho C_l^2\varepsilon_{xx} - 2\left(\mu R^2/\rho C_0^2\right)\varepsilon_{xxtt} = 0\,. \tag{23}$$

For the case of the steady propagation of shock wave, the single variable $\zeta = x - C_p t$ can be used. Eq. (23) takes the form:

$$(C_l^2 - C_p^2)\varepsilon_{\varsigma\varsigma} + 2\left(\mu R^2/\rho C_l^2\right)\varepsilon_{\varsigma\varsigma\varsigma\varsigma} = 0\,. \tag{24}$$

Exchanging $\varepsilon_{\varsigma\varsigma} = \psi$ leads to the equation for an oscillator:

$$(C_l^2 - C_p^2)\psi + 2\left(\mu R^2/\rho C_l^2\right)\Psi_{\varsigma\varsigma} = 0\,. \tag{25}$$

The frequency of oscillations equals

$$\omega = \frac{1}{2}\frac{\rho C_l^2 (C_l^2 - C_p^2)}{\mu R^2}. \quad (26)$$

Physically, the oscillatory regime of shock wave propagation is a sequence of *positive back coupling* provided by the Eqs. (1) and (13) which are used for locking the balance equations (14)-(17). The positive back coupling between macroscale and mesoscale is realized through the particle velocity dispersion and rate of its change.

As noted above, in our experiments the size of the laser spot of the interferometer (50-70 μm) at the free surface of the target corresponds to mesoscale-2 (50-500 μm) (see Fig. 1), so the experimental technique allows to registers: (i) the mean motion of *single structural element of mesoscale-2* as a whole and (ii) the fine structure of shock wave including the high-frequency oscillations at the mesoscale-2. The temporal resolution of experimental diagnostics (0.6-1.0 ns), allows registering the fine structure of plastic wave including the high-frequency oscillations at the mesoscale-2. Where observed, the oscillations are excited at the top of the plastic front. Figure 11 demonstrates the velocity oscillations in 7 mm 1565 aluminum alloy target loaded at the impact velocity of 636.5 m/s. The oscillations are seen at the impact velocities which are higher than the threshold of structure unstable transition, U_{inst}. The space period of oscillations equals ~ 50 μm, which coincides with the mean size fault-structures (40-50 μm). Thus, while the mesoscale-1 structures are nucleated owing to particle velocity pulsations, the fault-structures of mesoscale-2 are initiated due to resonance interaction of mesoscale-1 structures with the plastic front oscillations, which, in turn, result from positive back coupling between mesoparticle velocity dispersion (mesoscale) and velocity defect (macroscale).

Although oscillations are initiated due to the interaction of stochastic features of dynamically deformed structure in form of particle velocity dispersion, the transition itself happens *due to swinging* the high-frequency oscillations of mesostructure. Thus, it should be underlined that the macro-meso structural transition is *not a direct transition from the chaotic motion* of structural elements to *translation motion* of the next scale level as "noise-induced transition" [30]. This transition is thought to be realized through the oscillation regime of straining at the mesoscale. The oscillatory regime of dynamic deformation is found in shock-wave experiments with copper, Armco-iron, steels, and other materials. The example of oscillations in shock loaded 1565 aluminum alloy is provided in Fig. 11.

Below the dimensions of fault-structures are calculated for regions *AB* and *CD*. The experimental free surface profiles are used for the calculation of parameters of shock waves.

Region AB

1. Impact velocity U_{imp} = 335 m/s.
2. Velocity variance D = 22 m/s.
3. Velocity of plastic front $C_p = 5.478 \cdot 10^5$ cm/s.
4. Longitudinal sound velocity $C_l = 6.387 \cdot 10^5$ cm/s.
5. Strain rate $\frac{d\varepsilon}{dt} = 7.79 \cdot 10^5\ \mathrm{c}^{-1}$.
6. Shear modulus $\mu = 2.7 \cdot 10^{11} \frac{dyn \cdot cm}{sek^2}$.
7. Density ρ = 2.7 g/cm^3.

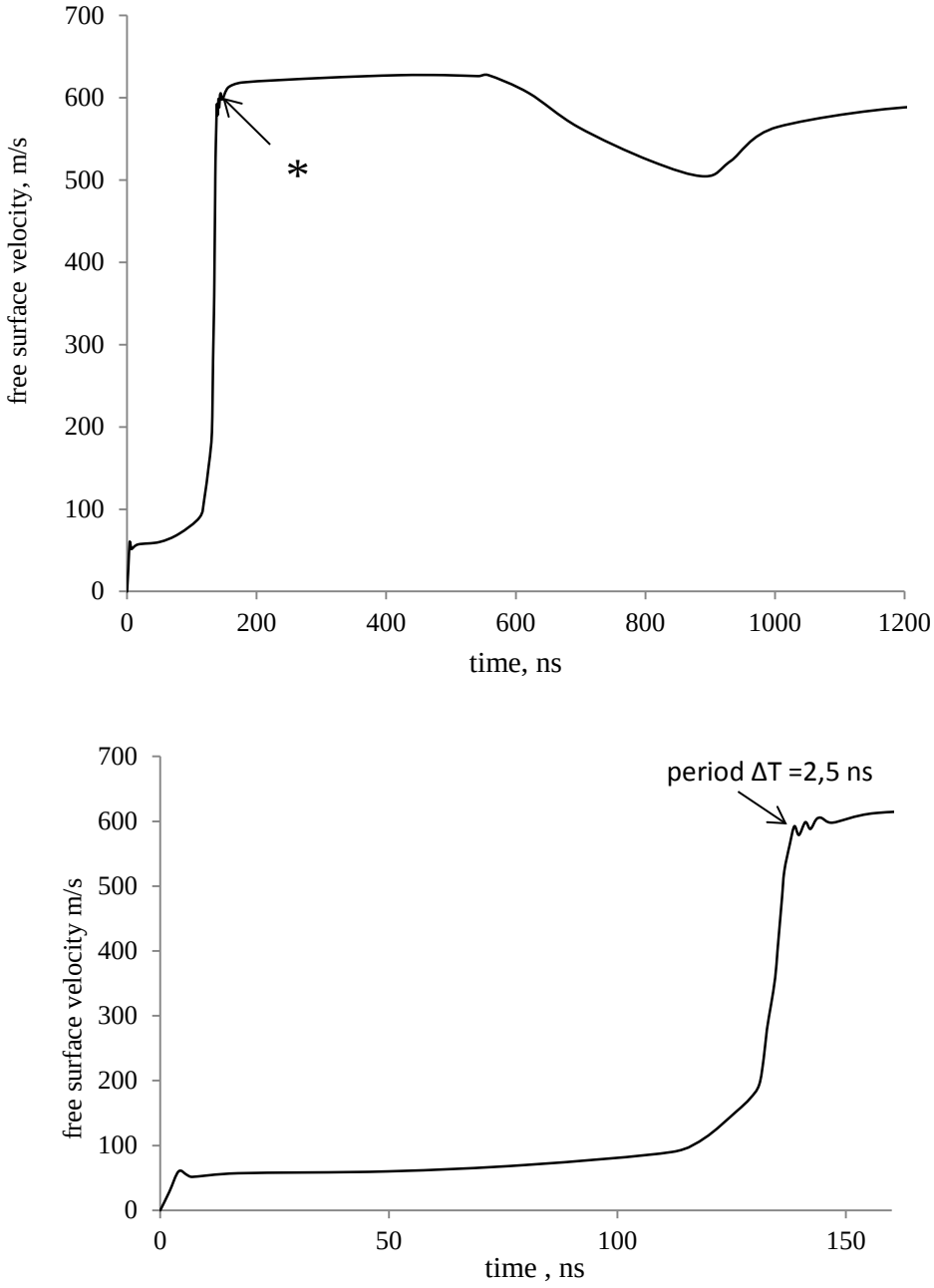

Fig. 11. Free surface velocity profiles, $u_{\text{fs,}}$ for 7 mm 1565 aluminum alloy target loaded at the impact velocity of 636.5 m/s (the oscillations are indicated by symbol *)

From Eq. (1) $R = \dfrac{D}{d\varepsilon / dt} = 28 \cdot 10^{-4}\, cm$ and from Eq. (26) $\omega = 2.35 \cdot 10^{8}\, s^{-1}$ or $f = \omega / 2\pi = 0.374 \cdot 10^{8}\, s^{-1}$ which corresponds to period of oscillations $T = \dfrac{1}{f} = 2.672 \cdot 10^{-8}\, s$.

Then the space period of cell-structures in region *AB* equals: $\lambda = T \cdot U_{imp} = 2.672 \cdot 10^{-8}\, s \cdot 3.35 \cdot 10^{4}\, cm / s = 8.95 \cdot 10^{-4}\, cm$. The obtained value for space period of oscillations coincides with the dimensions of fault-structures shown in Fig. 10*a*.

Region CD

1. Impact velocity U_{imp} = 653.7 m/s.
2. Velocity variance D = 52 m/s.

3. Velocity of plastic front $C_p = 5.66 \cdot 10^5$ cm/s.

4. Longitudinal sound velocity $C_l = 6.387 \cdot 10^5$ cm/s.

5. Strain rate $\frac{d\varepsilon}{dt} = 5 \cdot 10^6 \text{ s}^{-1}$.

6. Shear modulus $\mu = 2.7 \cdot 10^{11} \frac{dyn \cdot cm}{sek^2}$.

7. Density ρ =2.7 g/cm^3.

From Eq. (1) $R = \frac{D}{d\varepsilon / dt} = 10.36 \cdot 10^{-4}$ cm and from Eq. (26) $\omega = 1.84 \cdot 10^8 s^{-1}$ or $f = \omega / 2\pi = 0.29 \cdot 10^8 s^{-1}$ which corresponds to the time period of oscillations $T = \frac{1}{f} = 2.35 \cdot 10^{-8} s$. Then the dimension of fault-structures in region *CD* equals $\lambda = T \cdot U_{imp} = 2.35 \cdot 10^{-8} \cdot 6.637 \cdot 10^4 = 47 \cdot 10^{-4} cm$. The obtained value for space period of oscillations coincides with the dimensions of fault-structures for region *CD* shown in Fig. 10*c*.

6. Conclusions

Shock tests of 1565 aluminum alloy in two schemes of loading reveal the difference in mechanisms and scales of mesostructure formation depending on the scheme of shock loading and strain rate. Formation of fault-structures increases the resistance to high-velocity penetration. At the upper region of impact velocities, 1565 aluminum alloy reveals the increased resistivity to penetration.

Within impact velocity range of 250 - 750 m/s the strength behavior of alloy proves to be opposite – when resistance to penetration increases, the spall strength decreases.

The defect of particle velocity plays a role of a control parameter in the dynamic deformation of the material. It defines the transition from one scale to another.

The transition from one structural scale to another is realized through the excitation of mesoscale oscillations resulted from the back coupling between deformation processes at the macroscale and mesoscale.

The maximum dynamic strength is realized in the impact velocity range where the velocity defect equal to the velocity variance.

Acknowledgements. *No external funding was received for this study.*

References

[1] Makarov PV. Microdynamic theory of plasticty and failure of structurally inhomogeneous media. *Isvestiya Vysshikh Uchebnykh Zavedenii, Fizika.* 1992:4; 42-58. (In Russian)

[2] Makarov PV. Physical mesochanics approach in simulationof deformation and fracture processes. *Physical Mesomechnics.* 1981;1: 57-75.

[3] Baer MR, Trott WM. Mesosscale description of shock-loaded heterogeneous porous energetic materials. *Bulleten of the Amer Phys. Soc.* 2001;46(4): 102.

[4] Briant C, Morris B, Tombrello T, YIP S. In: *Repors of Bodega Bay Workshop on Multi-Scale Modeling of Materials.* 2001. p.7-10.

[5] Nesterenko VF. *Dynamics of Heterogeneous Materials*. New York: Springer; 2002.

[6] Kanel GI. *Shock waves in solid state physics*. CRC Press; 2019.

[7] Johnson JN, Jones OT, Michaels TE. Dyslocatiob dynamics and single-crystal constitutive relation: shock-wave propagation and precursor decay. *J. Appl. Phys*. 1970;41(6): 2230-2239.

[8] Meshcheryakov YI. Particle velocity non-uniformity and steady wave propagation. *Shock Waves, Detonation and Explosives.* 2016;26(3): 11-25.

[9] Buravova CN. *Etudes on localization of dynamic deformation.* Palmarium Academic Publishing; 2014. (In Russian)
[10] Vladimirov VI, Ivanov VN, Priemskii NM. Mesoscopic level of plastic deformation. In: Zhurkov SI. (Ed.) *Physics of Strength and Plasticity*. Moscow: Nauka;1986. p.69-80. (In-Russian)
[11] Eshby MF. The deformation plastically non-homogeneous materials. *Philosophical Magazine.* 1970;21(170): 399-422.
[12] Meshcheryakov YI, Prokuratova EI. Kinetic theory of continuously distributed dislocations. *International Journal of Solids and Structures.* 1995;3(12): 1711-1726.
[13] Prokuratova EI, Indeitzev DA. The conditions of the dislocation distributions localization under dynamic loading. *Dymat Journal.* 1995;2(3/4): 229-233.
[14] Chhabildas LC, Trott WM, Reinhart WD, Cogar IR, Mann GA. Incipient spall structures in tantalum- microstructural effects. In: Funish MD, Thadani NN, Horie YY. (Eds.) *Shock Compression of Condenced Matter-2001*. 2001. p.483-486.
[15] Baer MR. Computatinal modeling of heterogeneous reactive materials at the mesoscale. In: Furnish MD, Chhabildas LC, Nixon RS. (Eds.) *Shock compression of condenced matter-1999.* New York: The APS Proceedings; 1999. p.27-33.
[16] Vogler TJ, Reinhart WD, Chhabildas LC. Dynamic behavior of boron carbide *J. Appl. Phys.* 2004;95(8): 4173-4183.
[17] Yano K, Horie Y. Discrete-element modeling of shock compression of polycrystalline copper. *Phys. Rev. B.* 1999;59(21): 13672-13680.
[18] Case S, Horie Y. Discrete element simulation of shock wave propagation in polycrystalline copper. *Journal of the Mechanics and Physics of Solids*. 2007;55: 389-514.
[19] Asay JR, Barker LM. Interferometric measurements of shock-induced internal particle velocity and spatial variation of particle velocity. *J. Appl. Phys.* 1974;45(10): 2540-2546.
[20] Meshcheryakov YI, Divakov AK. Multiscale kinetics of microstructure and strain-rate dependence of materials. *Dymat Journal.* 1994;1(4): 271-277.
[21] Meshcheryakov YI, Divakov AK, Zhigacheva NI. Shock-induced structural transitions and dynamic strength of solids. *Int. Journ Solids and Structures.* 2004;41(9-10): 2349-2362.
[22] Meshcheryakov YI, Zhigacheva NI, Divakov AK, Makarevich IP, Barakhtin BK. Transition of metals into structure-unstable state under shock loading. *Prikladnaya Mechanika i Tekhnicheskaya FIzika.* 2010;51(5): 132-146. (In Russian)
[23] Meshcheryakov YI, Divakov AK, Zhigacheva NI, Makarevich IP. Dynamic structures in shock-loaded copper. *Physical Review. B.* 2008;78(6): 64301-64316.
[24] Khantuleva TA, Meshcheryakov YI. Nom-equilibrium processes in condensed media. Part 2. Shock-induced structural instability. *Phisical Mesomechanics*. 2005;8(6): 5-21.
[25] Cohran S, Banner D. Spall studis of uranium. *J. Appl. Phys.* 1977;48(7): 2729-2737.
[26] Indeitzev DA, Meshcheryakov YI, Kuchmin AY, Vavilov DS. Multiscale model of steady-wave shock in a medium with relaxation. *Acta Mechanica*. 2014;226(3): 917-925.
[27] Hintze T. *Turbulence.* NY: Graw Hill Inc; 1962.
[28] Duvall GE. Propagation of plane shock waves in a stress-relaxing medium In: Kolsky H, Prager W. (Eds.) *Shock Waves in Inelastic Solids*. Berlin: Springer; 1964. p.20-32.
[29] Taylor JW. Dislocation dynamics and dynamic yielding. *J. Appl. Phys.* 1965;36(10): 3146-3155.
[30] Horsthemke W, Lefever R. *Noise-Induced Transitions*. New York: Springer; 1984.